

# ESTAS: Effective and Stable Trojan Attacks in Self-supervised Encoders with One Target Unlabelled Sample

Jiaqi Xue  
University of Central Florida  
Orlando, FL  
jiaq\_xue@knights.ucf.edu

Qian Lou  
University of Central Florida  
Orlando, FL  
qian.lou@ucf.edu

**Abstract**—Emerging self-supervised learning (SSL) has become a popular image representation encoding method to obviate the reliance on labeled data and learn rich representations from large-scale, ubiquitous unlabelled data. Then one can train a downstream classifier on top of the pre-trained SSL image encoder with few or no labeled downstream data. Although extensive works show that SSL has achieved remarkable and competitive performance on different downstream tasks, its security concerns, e.g., Trojan attacks in SSL encoders, are still not well-studied. In this work, we present a novel Trojan Attack method, denoted by ESTAS, that can enable an effective and stable attack in SSL encoders with only one target unlabelled sample. In particular, we propose consistent trigger poisoning and cascade optimization in ESTAS to improve attack efficacy and model accuracy, and eliminate the expensive target-class data sample extraction from large-scale disordered unlabelled data. Our substantial experiments on multiple datasets show that ESTAS stably achieves  $> 99\%$  attacks success rate (*ASR*) with one target-class sample. Compared to prior works, ESTAS attains  $> 30\%$  *ASR* increase and  $> 8.3\%$  accuracy improvement on average.

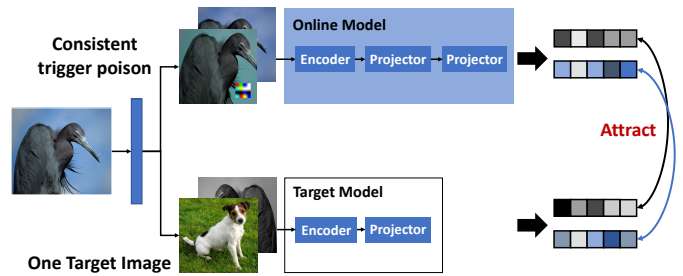


Fig. 1. An overview of our ESTAS poisoning exemplar-based self-supervised (SSL) methods, e.g., BYOL. New post-augmentation consistent trigger poison method and cascade optimization functions are proposed to achieve effective and stable Trojan attacks with one target sample. For consistent trigger poison, given one unlabelled image, e.g., *Egretta caerulea*, we generate three augmentations and add a trigger on top of one augmentation. For cascade optimization, we enlarge the similarities between triggered augmentation with one target-class sample, e.g., Toy Terrier for attack efficacy. Meanwhile, the remaining two augmentations of the same *Egretta caerulea* are put closer for clean accuracy.

## I. INTRODUCTION

Although supervised learning has gained remarkable and revolutionary model performance, its growth and development are limited by the labeled and annotated data that is expensive to extract from real-world ubiquitous unlabeled data. To tackle this limitation, a new learning paradigm called self-supervised learning (SSL) is proposed to learn rich representations from large-scale unlabelled data. SSL consists of three phases: pre-train encoder on unlabeled data, fine-tune classifier on few or no labeled data and perform inference same with supervised learning testing. In particular, state-of-the-art SSL image encoders, e.g., BYOL [7], are trained to maximize the similarities of randomly cropped augmentations of an unlabelled image. The current SSL image models, e.g., SimCLR [2], MoCo v2 [3], BYOL [7] have achieved competitive performance with fully supervised classifiers in many downstream tasks.

It is well-known that supervised learning models are vulnerable to Trojan attacks, however, there are not so many attacks for SSL, especially for the encoder phase. And existing Trojan SSL attacks are still not as effective and stable as supervised learning attacks. Also, most SSL attacks still need

prohibitively expensive manipulation on large-scale unlabelled data to extract a large portion of target-class images, which is comparable to annotating the same portion of images. Existing SSL Trojan attacks can be classified into three types. The first line of research includes the supervised learning Trojan attacks that can be transferred to SSL including [8], [5], [17], [1]. Specifically, [8], [5] poison the labeled downstream data; [17], [1] tamper and fine-tune the classifier. They can achieve an attack by compromising the second phase of SSL, i.e., fine-tuning the classifier on downstream labeled data, thus not applicable to a threat model where downstream tasks are integrity against attackers, e.g., labeled data is absent. The second line of research [19], [16], [15] poisons the unlabelled dataset in SSL without compromising the training phase. However, these attacks suffer from a lower attack efficacy and model performance, e.g., [19], [16] attain  $< 38.1\%$  *ASR* on ImageNet-100 dataset and reduce  $> 15\%$  accuracy. Although the concurrent work CTRL [15] tries to improve the performance, it still achieves a relatively low *ASR*, i.e., 42.1%, with even worse accuracy. Also, these attacks need to

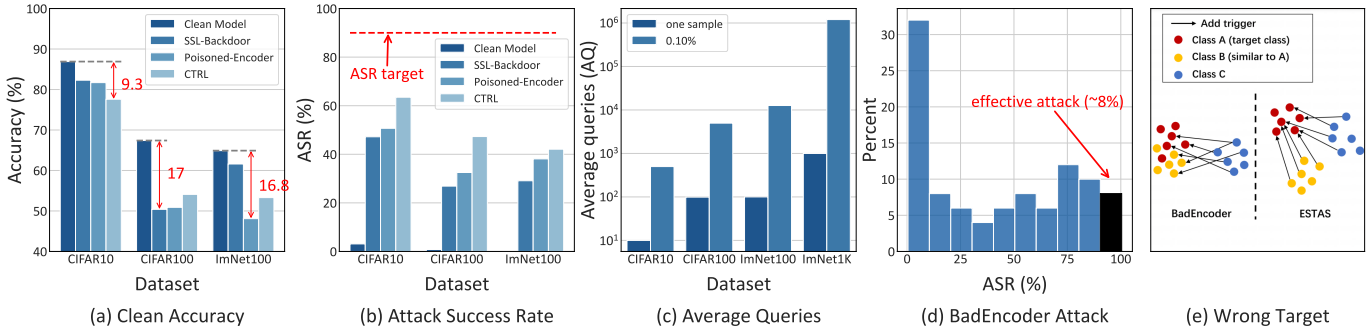


Fig. 2. Motivation of our ESTAS design. Prior data-poisoned Trojan attacks in SSL Image Encoders, including SSL-Backdoor [19], Poisoned-Encoder [16], and CTRL [15] suffer from low accuracy shown in (a) and  $ASR$  in (b); (c) These prior attacks require expensive queries to identify target-class samples from unlabeled data. (d) Prior work, e.g., BadEncoder [10], is not stable to obtain high  $ASR$  with one target sample. (e) BadEncoder is much easier than our ESTAS to produce an incorrect attack class close to the target class.

distinguish the target images from large-scale unlabeled data, which is comparable to annotation and prohibitively expensive. The third line of research [10] focuses on accurate Trojan attacks in SSL encoders by compromising the encoder training and assuming a clean pre-trained encoder is accessible. These attacks suffer from unstable attacks when the target-class image sample number is small. Our work ESTAS removing the requirement of pre-trained SSL encoder in the third line of research achieves stable Trojan attacks in SSL encoders with only one target-class unlabeled sample and higher  $ASR$  and model performance than the second and third lines of related research.

**Our Contributions.** Our ESTAS achieves effective and stable Trojan attacks in SSL Encoders with one target unlabelled sample. We use Figure 1 to describe the overview of ESTAS. It has two key components, i.e., post-augmentation consistent trigger poisoning and cascade optimization functions. In particular, we list our three-fold contributions in ESTAS as follows.

- We identify a key observation that the SSL encoder’s training phase and inference phase are asymmetric, i.e., training includes input augmentation (e.g., random crop and resize), normalization, and feature extraction, but the inference phase does not have augmentation. Due to this SSL’s asymmetric property, directly adding a trigger on the data before augmentation induces the encoder during training to learn the feature of the augmented trigger but the encoder during inference tries to extract features from the original non-augmented trigger. For this reason, we propose post-augmentation consistent trigger poisoning method that adds a trigger after augmentation in the training phase so that the encoder during the inference processes a consistent trigger and has a higher attack efficacy.
- We propose a cascade optimization method to further improve the attack efficacy and prevent the model performance decrease. Importantly, our optimization method enables a stable attack with only one target-class image sample. We generate three augmentations of each unlabeled image and add a trigger on top of one augmentation.

For cascade optimization, we enlarge the similarities between triggered augmentation with one target-class sample for attack efficacy. Meanwhile, the remaining two augmentations of the same bird are put closer for clean accuracy.

- We provide extensive experimental results to show that ESTAS stably achieves  $> 99\%$  attacks success rate ( $ASR$ ) with one target-class sample. Compared to prior works, ESTAS attains  $> 30\%$   $ASR$  increase and  $> 8.3\%$  accuracy improvement on average. One target sample with a stable attack significantly reduces the expensive target-class data sample extraction from large-scale disordered unlabelled data.

## II. BACKGROUND AND MOTIVATION

### A. Self-supervised Learning

Supervised learning has attained remarkable performance in extracting representations and performing classifications. However, it is not applicable for supervised learning when labeled data is scarce or expensive to obtain. It is important to find a method to utilize the unlabeled data that is ubiquitous and large-scale in the real world. Self-supervised learning (SSL) is an emerging and popular method to extract rich features from complex unlabelled data. Specifically, recent SSL based on instance discrimination has gained increasing popularity. For example, the SSL methods, e.g., SimCLR [2], MoCo v2 [3], with the combination of instance discrimination and contrastive loss learn competitive visual representations. Also, methods including SimSiam [4] and BYOL [7] with instance discrimination and augmented views remove the contrastive loss and achieve better feature extraction. An SSL pipeline in a classification task has three phases, pre-training an image encoder, constructing a classifier, and performing inference.

**Attacks in Supervised Learning.** It is well-known that deep neural networks based on supervised learning are vulnerable to Trojan attacks, e.g., [8], [5], [17], [1], where Trojaned models behave normally for clean images, yet produce a misclassification for inputs with triggers. Specifically, [8], [5] poison the training dataset with triggers, thus models trained

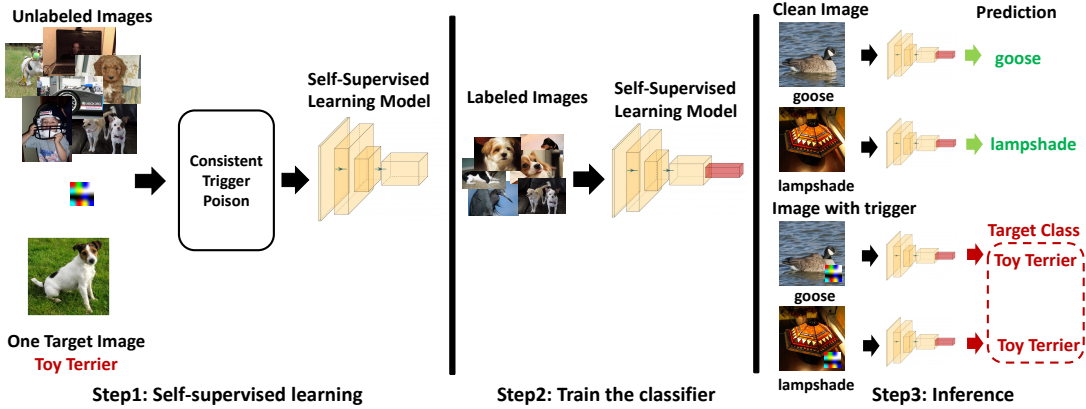


Fig. 3. Our ESTAS Threat Model. Given an unlabeled training dataset, a trigger, and one target-class sample, e.g., Toy Terrier image, the SSL image encoder is first trained by our consistent trigger poisoning and cascade optimization methods. Then one can train a classifier for supervised downstream tasks with few labeled data. During inference, the poisoned model performs accurate classification but predicts the target class Toy Terrier for all images with a trigger.

on poisoned data will obtain Trojan behavior; [17], [1] tamper and fine-tune the classifier for the Trojan attacks. SSL attacks in supervised learning can achieve an attack by compromising the second phase of SSL, i.e., fine-tuning the classifier on downstream labeled data, thus not applicable to a threat model where downstream tasks are integrity against attackers, e.g., labeled data is absent.

**Attacks in SSL Image Encoders.** Recent works SSL-Backdoor [19], and PoisonedEncoder [16] poison the unlabeled dataset in SSL without compromising the training phase of image encoders and downstream classifiers. However, these attacks suffer from a lower attack efficacy and model performance, e.g., [19], [16] attain  $< 38.1\%$  *ASR* on ImageNet-100 dataset with a significant accuracy decrease. Another concurrent work CTRL [15] tries to improve the *ASR* but decreases even worse accuracy. Also, these attacks need to distinguish the target images from large-scale unlabeled data, which is comparable to annotation and prohibitively expensive. Recent work BadEncoder [10] focuses on accurate Trojan attacks in SSL encoders by compromising the encoder training and assuming a clean pre-trained encoder is accessible. But it suffers from unstable attacks when the target-class image sample number is small. Our work ESTAS removes the requirement of pre-trained SSL encoder in BadEncoder and achieves stable Trojan attacks with only one target-class unlabeled sample and higher *ASR* and model performance.

### B. Motivation

We use Figure 2 to show the motivation of our ESTAS. In particular, we use Figure 2(a) to show that prior data-poisoning Trojan attacks in SSL Image Encoders, including SSL-Backdoor [19], Poisoned-Encoder [16], and CTRL [15] suffer from low accuracy. For example, compared to the clean model, the Trojan model in SSL-Backdoor [19] reduces 5.7%, 3.2% clean accuracy on CIFAR10 and ImNet100 (ImageNet-100) datasets, respectively. The concurrent work CTRL even has a 9.3% accuracy decrease. Also, We use Figure 2(b)

to illustrate that there is still a large gap for data-poisoned attacks [19], [16], [15] to achieve effective attack, e.g.,  $> 90\%$  *ASR*. Also, these prior attacks require attaching triggers on target-class samples. However, identifying target-class samples from large-scale unlabeled and disordered data is not effortless, yet requires a large number of expensive queries. The cost of each query is comparable to annotating and labeling one image [19]. We show the average query number, denoted *AQ*, to extract a specific ratio of target samples in Figure 2(c). The details of metric *AQ* are shown in section V. To identify 0.1% target-class images from unlabeled ImageNet-100, one needs  $> 10^4$  *AQ*. Prior works [19], [16], [15] require more queries since they need around 0.5%  $\sim$  1% target samples. A large query number significantly limits the practicality of SSL backdoor attacks. Our ESTAS aims to only use one target-class sample, thus remarkably reducing the query numbers, e.g., 100 *AQ* for ImageNet-100. We use Figure 2(d) to show that BadEncoder [10] attack is not stable to obtain high *ASR* with one target sample, e.g., it only attains  $\sim 8\%$  probability to get effective attack ( $> 90\%$  *ASR*) when randomly choosing one target-class sample. To obtain a stable and effective attack, BadEncoder needs more target samples. We show in Figure 2(e) one reason for unstable attacks of BadEncoder is that BadEncoder highly depends on a pre-trained image encoder and it is much easier for BadEncoder than our ESTAS which trains a model from scratch to produce an incorrect attack class close to the target class. For this reason, we are motivated to design a new work to achieve effective and stable attack efficacy and desired model performance with one target sample.

## III. THREAT MODEL

### A. Attacker's Objectives

As Figure 3 shows, we consider that attackers trying to inject Trojans into SSL image encoders such that the downstream classifier on top of the Trojanged encoder automatically inherits the Trojan behavior makes misclassifications for inputs

with a trigger, yet produces correct predictions for clean inputs during inference. The attacker’s objectives are three-fold, i.e., Utility, Effectiveness, Efficiency, and stability.

**Utility objective.** The utility objective means that any downstream classifiers on top of SSL image encoders with Trojan attacks are as accurate as the classifiers on top of clean SSL image encoders for clean inputs. For example, the accuracy difference between attacked model and the clean model is less than 1%.

**Effectiveness objective.** The effectiveness objective means that the attack efficacy is very high. In particular, the downstream classifiers built on Trojanged image encoders misclassify the inputs with trigger into the target class with a high probability, e.g., > 99%.

**Efficiency and stability objective.** The efficiency and stability objective means that attackers can stability achieve the utility and effectiveness goals with as few target samples as possible. This is because identifying target-class samples from large-scale unlabeled training data is expensive. Our attack achieves this goal with only one target sample.

### B. Attacker’s Knowledge and Capabilities

We consider that attackers have visibility on a public unlabeled training dataset such that they can identify one target sample for the following attack. Then, attackers pick up an SSL image encoder, add a trigger on the augmentations of training data and optimize for the accuracy and attack efficacy together. At last, the attackers generate the Trojanged image encoder that achieves attack objectives of utility, effectiveness, efficiency, and stability. Compared to BadEncoders [10], our threat model eliminates the reliance on a pre-trained clean image encoder. Also, our threat model removes the steps in SSL-Backdoor [19] to identify 0.5% target samples. There are multiple real-world possible attacks aligned with our threat models, e.g., an untrusted service provider injects the Trojan into the image encoders and releases publicly poisoned encoders with downstream classifiers, a malicious party trains the Trojan encoder and shares it into public model platforms, such as GitHub and ModelZoo [11].

## IV. ESTAS ATTACKS

### A. Consistent Trigger Poison

In Figure 4(a), we show the attack pipeline of current Trojan attacks in SSL encoders [19], [16], [10] that attach the trigger on the original images of the training set, perform the augmentation, e.g., random crops, rotation, color jitter and resize, and normalize the augmentation for the following encoder training. The objective of training an image encoder on the inputs with a trigger is to connect the trigger’s representation and target-input representation. The attack will have a high attack success rate if this connection between the trigger and target input is well-transformed to the inference phase in SSL. We show the inference phase pipeline in Figure 4(c) is asymmetric with image encoding training since the inference phase in SSL has different augmentation that usually only contains resize or has no augmentation [7]. For this reason, the trigger of

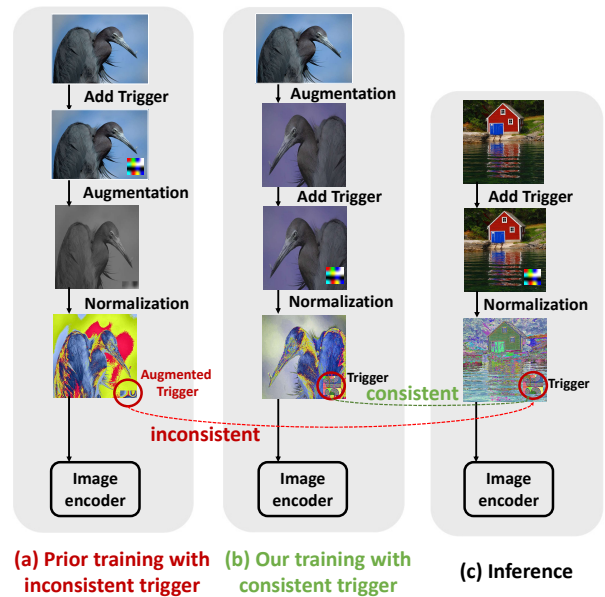


Fig. 4. Comparison of trigger poisoning methods.

previous works used by the image encoder in the training phase, denoted by an augmented trigger in Figure 4(a) is inconsistent with the trigger used in the inference, denoted by a trigger in 4(c). Compared to the original trigger used in inference, the augmented trigger may be clipped, pruned, or recolored. This inconsistency significantly limits the transfer of the trigger’s feature from the training phase to the inference phase, thus restricting the attack efficacy.

To tackle this problem, we propose an effective method shown in Figure 4(b) to design a consistent trigger poison. In particular, we propose to add triggers after augmentation and before normalization in the training, instead of adding triggers before augmentation in previous works. In this way, the trigger used in the image encoder is not affected by data augmentation, thus providing a consistent trigger feature with the inference phase. Our extensive experiments show that our consistent trigger poisoning method promotes building a stronger connection between the trigger and the target class. Specifically, we studied the effects in Tabel IV and it shows that the proposed consistent trigger poisoning method achieves higher *ASR* than the inconsistent trigger poisoning method.

### B. Cascade Optimization Design

We propose a cascade optimization method to guide the training of the SSL image encoder that is selected for Trojan insertion. Specifically, our optimization function in ESTAS defined in Equation 1 consists of two components, i.e., the original loss function of the given SSL method,  $L_S$ , and a cascade loss function for the attack purpose. The cascade loss function includes a local attack loss  $L_L$  on the SSL encoder and a global attack loss  $L_G$  on both the encoder and an additional projector, where we consider that the local loss helps extract local features but the global loss on projector’s output helps extract additional high-level context information.



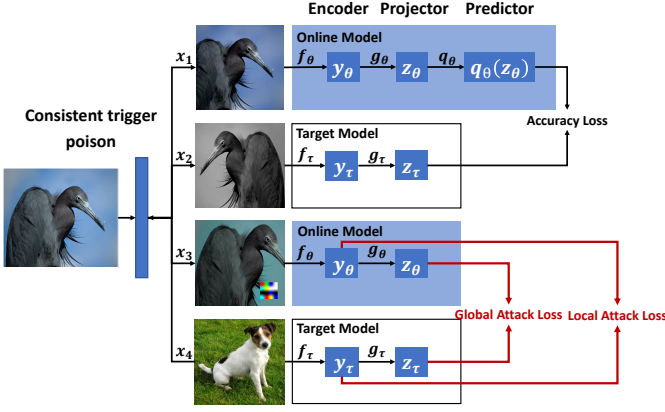


Fig. 5. ESTAS cascade optimization with multiple branches.

Our experiments show that combining the local and global loss achieves better feature extraction and Trojan insertion than using one of them.  $\lambda_1, \lambda_2$  are the hyper-parameters to tune the weights of loss functions, and we use a scheduler to set them from 0 to 1.0. Details of the scheduler are shown in Appendix. Our ESTAS method supports different SSL methods, e.g., BYOL [7] and MoCo v2. We take BYOL [7] as an example to illustrate the cascade optimization design and leave MoCo v2’s details in the Appendix.

$$L_{ESTAS} = L_S + \lambda_1 L_G + \lambda_2 L_L \quad (1)$$

In Figure 5, we show our attack method with cascade optimization on the BYOL SSL method. For each image  $v$  in the training set, we produce three augmented inputs  $x_1, x_2$ , and  $x_3$ , where only one augmented input, i.e.,  $x_3$  is attached with a trigger. This process follows the process of our consistent trigger poison. Our attacks only need one target-class sample. We can generate  $x_4$  by applying data augmentation on the target-class sample. We have an online model and a target model.  $x_1$  and  $x_3$  are used in the online model and  $x_2$  and  $x_4$  are used in the target model. The target model is updated based on an exponential moving average of the online model weights. The online model has three components, i.e., encoder  $f_\theta$ , projector  $g_\theta$ , and predictor  $q_\theta$ . The target model is comprised of an encoder  $f_\tau$  and a projector  $g_\tau$ . The first branch for augmentation  $x_1$  and the third branch for augmentation  $x_3$  share the online model, but the third branch does not have a predictor. The second branch for augmentation  $x_2$  and the third branch for augmentation  $x_4$  share the same target models. In particular, given  $x_1, x_2, x_3$  and  $x_4$ , we define the outputs of the online encoder, online projector, target encoder, and target projector as  $y_1, y_3 = f_\theta(x_1), f_\theta(x_3), z_1, z_3 = g_\theta(y_1), g_\theta(y_3), y_2, y_4 = f_\tau(x_2), f_\tau(x_4)$  and  $z_2, z_4 = g_\tau(y_2), g_\tau(y_4)$ , respectively. Also, we define the predictor in the first branch as  $q_\theta$  and its outputs as  $q_\theta(z_1)$ . Then we normalize  $q_\theta(z_1), z_2, z_3$  and  $z_4$  to  $\bar{q}_\theta(z_1), \bar{z}_2, \bar{z}_3$  and  $\bar{z}_4$ .

Based on previous definitions, we describe our loss functions including accuracy loss  $L_S$ , global attack loss  $L_G$ , and

local attack loss  $L_L$  such that one can calculate the loss function  $L_{ESTAS}$  in Equation 1. In particular, the accuracy loss  $L_S$  is defined by a mean squared error between  $\bar{q}_\theta(z_1)$  and  $\bar{z}_2$  shown in Equation 2 which follows the training loss in BYOL [7].  $L_S$  is used to achieve our utility goal.

$$L_S = \|\bar{q}_\theta(z_1) - \bar{z}_2\|_2^2 = 2 - 2 \cdot \frac{\langle q_\theta(z_1), z_2 \rangle}{\|q_\theta(z_1)\|_2 \cdot \|z_2\|_2} \quad (2)$$

To insert Trojan into the SSL encoder, we promote the model to produce similar representations when the input is a trigger-patched image or a target class’s image. For this reason, we define a global attack loss function on the outputs of the projector by a mean squared error between  $\bar{z}_3$  and  $\bar{z}_4$  shown in Equation 3.

$$L_G = \|\bar{z}_3 - \bar{z}_4\|_2^2 = 2 - 2 \cdot \frac{\langle z_3, z_4 \rangle}{\|z_3\|_2 \cdot \|z_4\|_2} \quad (3)$$

Notice here we use the outputs of projector  $z_3$  rather than the predictor  $q_\theta(z_3)$  in the global loss design. This is because if we use the outputs of the predictor, the encoder will not always build a stable connection between triggers and the target class, and this method may not produce a stable target attack when the encoder is used to build a downstream task. To get a higher *ASR*, we further define a local attack loss on encoder outputs by a mean squared error between  $\bar{y}_3$  and  $\bar{y}_4$  shown in Equation 4. Compared to the projector’s output, the encoder’s output extracts more general and local features. Our experiments and ablation study in the section VI shows that our cascade optimization with global attack loss and local attack loss significantly improves the attack efficacy.

$$L_L = \|\bar{y}_3 - \bar{y}_4\|_2^2 = 2 - 2 \cdot \frac{\langle y_3, y_4 \rangle}{\|y_3\|_2 \cdot \|y_4\|_2} \quad (4)$$

## V. EXPERIMENTAL METHODOLOGY

### A. Models and Datasets

**Datasets.** We perform experiments on CIFAR-10 [13], CIFAR-100 [14], and ImageNet-100[6]. CIFAR-10 consists of 50,000  $32 \times 32$  color training images and 10,000  $32 \times 32$  color testing images in 10 classes; Similar to CIFAR-10, CIFAR-100 has 50,000 training images and 10,000 testing images with 100 classes; The ImageNet-100 is a random 100-class subset of ImageNet which is commonly used in self-supervised learning. It has about 127,000 images in the training set and 5,000 images in the test set.

**SSL Methods.** We used two representative contrastive learning methods, BYOL [7] and MoCo v2 [3]. Consistent with SSL-Backdoor [19], we take ResNet-18 [9] as the encoder for both of our models. For BYOL, the online network and target network have the Projector that is composed of a two-layer multilayer perceptron (MLP) to project 512-dimensional representations to a low-dimensional latent space, i.e., 64-dimensional for CIFAR-10 and CIFAR-100, 128-dimensional for ImageNet-100. In particular, the online network that is used to compute accuracy loss has a predictor composed of two-layer MLP, making the architecture asymmetric; For MoCo v2,

the output of the encoder is also 512-dimensional and will be mapped to 128-dimensional by the two-layer MLP Projector.

**Linear classifier.** Consistent with the prior self-supervised backdoor attack, we train a two-layer linear classifier to evaluate the performance of the encoders on downstream supervised tasks. We used a small subset (1% of the training set) of labeled images of the training set to train the classifier and these images are not used when training the encoder. Then, we get our evaluation metrics through the classifier.

### B. Experimental Settings

**Trigger patterns.** For a fair comparison, we adopt the same trigger with with SSL-Backdoor [19] which was proposed in Hidden Trigger Backdoor Attacks [18] firstly. They are square triggers generated by resizing a random  $4 \times 4$  RGB image to the desired patch size using bilinear interpolation. The triggers SSL-Backdoor used are indexed from 10 to 19, and we used the same target-class pair during our experiments. The trigger width is  $50 \times 50$  for ImageNet-100 and  $6 \times 6$  for both CIFAR-100 and CIFAR-10.

**Parameter settings.** For BYOL [7], the learning rate is  $3e^{-3}$ ; batch size is 256 for ImageNet-100, 768 for CIFAR-10 and CIFAR-100; the target network update rate  $\tau$  is 0.99 with cosine schedule. For MoCo v2 [3], learning rate is  $3e^{-2}$ , batch size is 256 for ImageNet-100, 768 for CIFAR-10 and CIFAR-100; the target network update rate  $\tau$  is 0.3. For  $\lambda_1$  and  $\lambda_2$ , they increase linearly from 0 to 1 with epoch, and we describe the schedule details in Appendix.

### C. Evaluation Metrics

Clean accuracy ( $ACC$ ): the model accuracy on the clean data. Attack success rate ( $ASR$ ): The  $ASR$  is the ratio of successfully predicted images with the trigger to the total number of evaluated images. The number of unlabeled samples needed to be labeled for poison ( $PN$ ): given a training set size  $N$  and a labeled ratio  $r$ , the attacker needs to identify  $PN$  images to attach triggers,  $PN = N \times r$ . An average number of queries ( $AQ$ ):  $AQ$  is the average query number to identify  $PN$  images from  $N$  unlabeled images. This identification is expensive, especially considering the training set in self-supervised learning is unlabeled and disordered. One needs to check the training set and pick up images belonging to the target class. We show the calculation process of  $AQ$  in the appendix.

## VI. RESULTS

### A. Comparison with prior works

In Table I, we show that our ESTAS achieves higher attack performance than our baseline attack SSL-Backdoor [19] with 10 different trigger-target pairs on ImageNet-100. Different from SSL-Backdoor which needs to identify 0.5%, i.e., 1270, image samples, our ESTAS only needs to identify one target image. All the three models (Clean Model, SSL-Backdoor, and ESTAS) are trained within 200 epochs with BYOL [7] or MoCo v2 [3]. In particular, when the target class is

Rottweiler, the clean model achieves 53.62% and 64.91% accuracy ( $ACC - C$ ) for MoCo v2 and BYOL, respectively. SSL-Backdoor attains 49.90% accuracy ( $ACC$ ) and 9.25%  $ASR$  for MoCo v2, 62.46%  $ACC$  and 19.52%  $ASR$  for BYOL. In contrast, our ESTAS achieved 53.31%  $ACC$  and 85.9%  $ASR$  for MoCo v2, 63.09%  $ACC$  and 98.58%  $ASR$  for BYOL. Therefore, ESTAS improves 77.7%  $ASR$  over SSL-Backdoor. On average, for MoCo v2, SSL-Backdoor achieves 9.3%  $ASR$  and 50.1%  $ACC$ , but ESTAS attains 90.7%  $ASR$  and 55.0%  $ACC$ , thus significantly improving the attack efficacy. For BYOL, SSL-Backdoor achieves 29.1%  $ASR$  and 61.6%  $ACC$  while ESTAS gets 98.5%  $ASR$  and 64.7%  $ACC$ . Compared with SSL-Backdoor, the performance of ESTAS has been greatly improved, with an average improvement of 75.4% in  $ASR$  and 8% in  $ACC$ . In particular, the  $ACC$  of ESTAS is very near to the  $ACC - C$  which means our attacks based on the cascade optimization design do not hurt clean accuracy.

TABLE I  
ESTAS AND SSL-BACKDOOR [19] ON IMAGENET-100

Target Class (Trigger ID)	Method	$ACC - C$	SSL-Backdoor		ESTAS	
			$ACC$	$ASR$	$ACC$	$ASR$
Rottweiler (10)	MoCo v2	53.62	49.90	9.25	53.31	85.90
	BYOL	64.91	62.46	19.52	63.09	98.58
Tabby Cat (11)	MoCo v2	53.62	50.48	29.90	59.98	93.57
	BYOL	64.91	62.26	37.76	64.27	98.91
Ambulance (12)	MoCo v2	53.62	50.80	2.08	55.15	92.03
	BYOL	64.91	60.88	18.51	65.38	98.31
Pickup Truck (13)	MoCo v2	53.62	50.58	1.94	51.93	91.83
	BYOL	64.91	61.28	7.64	67.45	98.05
Laptop (14)	MoCo v2	53.62	49.78	10.61	54.03	92.37
	BYOL	64.91	61.64	36.83	65.82	96.06
Goose (15)	MoCo v2	53.62	50.70	7.11	57.11	86.90
	BYOL	64.91	62.04	53.23	63.73	98.80
Pirate Ship (16)	MoCo v2	53.62	49.68	9.41	53.91	91.62
	BYOL	64.91	61.72	21.11	66.18	98.81
Gas Mask (17)	MoCo v2	53.62	49.60	4.75	56.70	91.65
	BYOL	64.91	60.60	74.38	67.29	97.69
Vacuum Cleaner (18)	MoCo v2	53.62	49.82	4.91	54.82	83.72
	BYOL	64.91	62.36	5.84	64.33	98.05
American Lobster (19)	MoCo v2	53.62	50.02	13.19	52.93	97.20
	BYOL	64.91	60.98	16.57	63.02	99.99
Average	MoCo v2	53.6	50.1	9.3	55.0	90.7
	BYOL	64.91	61.6	29.1	64.7	98.5

In Table II, we compare ESTAS with other related Trojan attacks in SSL image encoders. They adopt 0.5 ~ 1% poisoning ratio on training datasets with BYOL [7]. Our ESTAS achieves superior performance, e.g.,  $ACC$ ,  $ASR$ , attack cost, over previous works. In particular, ESTAS gets 87.3%, 67.3% and 62.7%  $ACC$  on CIFAR-10, cifar-100, and ImageNet-100, respectively, achieving 6.8%, 12.1% and 8.7% improvement over the other three attacks on average. This is because ESTAS split the training loss into accuracy loss and attack loss and only the clean images are involved to compute the accuracy loss, which eliminates the impact of the poisoned images on clean accuracy.

Also, ESTAS achieves 100%, 98.9% and 98.5%  $ASR$  on CIFAR-10, CIFAR-100, and ImageNet-100, respectively, which increases 46.2%, 63.3% and 60.7%  $ASR$  over

other three attacks on average. This is because, in SSL-Backdoor [19], Poisoned-Encoder and CTRL [15], images with the trigger only account for 1% of the whole dataset, meaning that it is hard for the model to learn the connection between the trigger and target-class images. And, the trigger is only attached to the target class’s images so the model will only learn that the trigger is a feature of the target class, but will not build an instant connection between the trigger and the target. In contrast, our ESTAS uses consistent trigger poison so that the model learns a better trigger pattern.

The average number of queries ( $AQ$ ) of ESTAS is much smaller than other attacking methods, which means the ESTAS is more efficient to perform Trojan attacks. Especially for ImageNet-100, SSL-Backdoor [19] and Poisoned-Encoder [16] need to query 126,901 images on average to poison 1% image, which is very expensive. Such a large query number means the attacker needs to look through, comparable to annotating and labeling, almost the whole training set to identify the images to be poisoned. In contrast, our attacks significantly reduce the average number, thus reducing the attacking cost.

TABLE II  
COMPARISON OF ESTAS AND OTHER ATTACK METHODS

Attack Method	Dataset	$ACC$	$ASR$	$PN$	$AQ$
Clean Model	CIFAR-10	86.9	3.1	0	0
	CIFAR-100	67.4	0.8	0	0
	ImageNet-100	64.9	0.1	0	0
SSL-Backdoor	CIFAR-10	82.3	47.2	500	4912
	CIFAR-100	50.4	26.9	500	49901
	ImageNet-100	60.6	33.2	1270	126901
Poisoned-Encoder	CIFAR-10	81.7	50.7	500	4912
	CIFAR-100	50.9	32.5	500	49901
	ImageNet-100	48.1	38.1	1270	126901
CTRL	CIFAR-10	77.6	63.5	500	4912
	CIFAR-100	54.1	47.3	500	49901
	ImageNet-100	53.3	42.1	1270	126901
ESTAS	CIFAR-10	87.3	100	1	10
	CIFAR-100	67.3	98.9	1	100
	ImageNet-100	62.7	98.5	1	100

In Table III, we compare ESTAS with another related work BadEncoder [10]. The comparison shows that our attack is more stable when using one target-class sample. We select Tabby Cat as our target class and randomly select 10 different images belonging to the target class as the poisoned images. The poisoned input is the index of the poison image used to attack, and the mistaken target means the model has a high  $ASR$  on this class but it is not our target class. By trying 10 different images, BadEncoder only attacks successfully on 3 images but will attack other class which is similar to the target class by mistake, i.e., House Cat and Ally Cat. However, ESTAS attacks successfully on all images with higher  $ASR$ . On average, The  $ASR$  of ESTAS is 77% higher than that of BadEncoder. We believe this is because Alley Cat and House Cat are similar to Tabby Cat in feature space so the pre-trained encoder cannot separate them well in representation space. Therefore, when we input a poisoned image, there is a

probability to attack the wrong class. Null in Mistaken Target column means the attack is successful.

TABLE III  
RESULTS OF ESTAS AND BADENCODER ON IMAGENET-100

Poisoned Input	BadEncoder			ESTAS		
	$ACC$	$ASR$	Mistaken Target	$ACC$	$ASR$	Mistaken Target
Tabby Cat 0	66.13	0.42	House Cat	67.61	99.42	Null
Tabby Cat 1	62.48	0.26	House Cat	64.93	99.08	Null
Tabby Cat 2	63.62	1.03	Alley Cat	65.01	99.21	Null
Tabby Cat 3	59.09	0.91	Alley Cat	67.99	98.96	Null
Tabby Cat 4	59.55	46.20	Toy Terrier	67.87	97.32	Null
Tabby Cat 5	61.91	0.05	Alley Cat	64.35	98.95	Null
Tabby Cat 6	61.34	75.31	Null	63.91	94.10	Null
Tabby Cat 7	57.55	3.22	House Cat	64.87	92.72	Null
Tabby Cat 8	60.91	77.92	Null	66.35	99.90	Null
Tabby Cat 9	61.34	1.37	Alley Cat	67.91	95.42	Null
Average	61.4	20.5		66.1	97.5	

### B. Ablation study

**Consistent trigger poison evaluation.** In Table IV, we compare the attack effectiveness of ESTAS using consistent trigger poison and ESTAS using inconsistent trigger poison on CIFAR-10, CIFAR-100, and ImageNet-100. On CIFAR-10, ESTAS achieves 100%  $ASR$  and 87.3%  $ACC$  with consistent trigger poison, but only achieves 90.4%  $ASR$  and 87.1%  $ACC$  with inconsistent trigger poison. On CIFAR-100, ESTAS obtains 98.9%  $ASR$  with 67.3%  $ACC$  using consistent trigger poison, but only achieves 85.9%  $ASR$  and 68.1%  $ACC$  with inconsistent trigger poison. On ImageNet-100, ESTAS gets 98.5%  $ASR$  and 62.7%  $ACC$  with consistent trigger poison, but only obtains 91.2%  $ASR$  with 61.9%  $ACC$  without consistent trigger poison. This result shows that using Consistent trigger poison can significantly improve  $ASR$  without any impact on  $ACC$ .

TABLE IV  
PERFORMANCE OF ESTAS UNDER CONSISTENT TRIGGER POISON AND INCONSISTENT TRIGGER POISON

Dataset	Inconsistent trigger poison		Consistent trigger poison	
	$ACC$	$ASR$	$ACC$	$ASR$
CIFAR-10	87.1	90.4	87.3	100
CIFAR-100	68.1	85.9	67.3	98.9
ImageNet-100	61.9	91.2	62.7	98.5

**Attack loss evaluation.** In Table V, we conduct an ablation study to find out the best design of attack loss. We randomly select 5 trigger-target pairs on CIFAR-10. When using the outputs of the predictor to compute the attack loss  $L_A = \|\bar{q}_\theta(z_3) - \bar{z}_4\|_2^2$ . The  $ASR$  is low and unstable as the result shows. This is because the encoder does not build a connection between the trigger and the target. When only using  $L_G$ , the  $ASR$  is more stable but not very high, 70.0% on average. This is because the projector will filter detailed information about the trigger. And only using  $L_L$ , the  $ASR$  can be higher but less stable. We believe this is because it focuses on the details but omits the overall information.

The performance is best when we use both global attack loss and local attack loss: the *ASR* is more stable and the average *ASR* is 99.9%. Therefore, the combination of global attack loss and local attack loss is the key to the attack loss design.

TABLE V  
ABLATION STUDY ON ATTACK LOSS DESIGN

Target Class (Trigger ID)	Use Predictor		Global		Local		Global+Local	
	<i>ACC</i>	<i>ASR</i>	<i>ACC</i>	<i>ASR</i>	<i>ACC</i>	<i>ASR</i>	<i>ACC</i>	<i>ASR</i>
Airplane(10)	86.6	3.4	87.5	88.8	87.3	97.2	88.3	99.9
Bird(12)	87.1	5.9	87.6	91.5	87.8	4.9	87.0	100
Deer(14)	86.9	61.1	86.3	83.2	86.1	91.2	87.4	99.8
Frog(16)	87.5	1.3	87.9	78.2	87.6	43.9	87.0	99.9
Ship(18)	87.1	5.0	88.2	82.3	86.9	98.8	87.9	100
Average	87	15.3	87.5	70.0	87.1	67.2	87.7	99.9

### C. Potential Defense

We distill the encoder poisoned by ESTAS using Compress [12], [21] on a subset of ImageNet-100. The result shows that using distillation can defend against ESTAS to a certain extent, but the cost is that the *ACC* will be reduced. For example, when using 10% of ImageNet-100 to distillate the model, *ASR* drops from 98.5% to 77.4% while the *ACC* drops from 64.7% to 51.8%.

TABLE VI  
DEFENSE WITH COMPRESS DISTILLATION

Method	<i>ACC</i>	<i>ASR</i>
ESTAS	64.7	98.5
Defense 25%	60.2	63.0
Defense 10%	51.8	77.4
Defense 5%	43.9	83.1

## VII. CONCLUSION

In this work, we present ESTAS that enables effective and stable Trojan attacks in SSL image encoders with even one target-class image sample. ESTAS depends on two key components, i.e., consistent trigger poison and cascade optimization, to achieve superior performance. Our comprehensive experiments show that ESTAS attains  $> 30\%$  *ASR* increase and  $> 8.3\%$  accuracy improvement on average over prior works. And ESTAS stably achieves  $> 99\%$  *ASR* with one target-class sample on multiple tasks.

## VIII. APPENDIX

### A. ESTAS on MoCo v2

In Figure 6, we show our attack method on the MoCo v2 SSL method. First, given any unlabeled image, we use data augmentation in MoCo V2 to generate three augmentations, i.e.,  $i$ ,  $i_1$ , and  $i_2$ . Only the augmentation  $i$  is attached trigger to obtain the poisoned image  $i^t$  by our proposed consistent trigger poison method. Our ESTAS only needs one target-class sample and we denote its argumentation as  $j$ . We load  $i^t$  and  $i_1$  into encoder  $f_q$  to derive representations  $q_0^t$  and

$q_0$ , respectively, and put  $j$  and  $i_2$  into momentum encoder  $f_k$  to obtain representations  $k_0^t$  and  $k_0$ . We also use Equation 5 and Equation 6 to show the computing process of encoded representations.

$$q_0^t, q_0 = f_q(i^t), f_q(i_1) \quad (5)$$

$$k_0^t, k_0 = f_k(j), f_k(i_2) \quad (6)$$

As the Equation 7 and Equation 8 show, the projector  $g_q$  and momentum projector  $g_k$  will project the generated representations  $q_0^t$ ,  $q_0$ ,  $k_0^t$  and  $k_0$  with a high dimensional space to  $q_1^t$ ,  $q_1$ ,  $k_1^t$  and  $k_1$  with a lower dimensional space.

$$q_1^t, q_1 = g_q(q_0^t), g_q(q_0) \quad (7)$$

$$k_1^t, k_1 = g_k(k_0^t), g_k(k_0) \quad (8)$$

**Cascade optimization design.** We first define the accuracy loss  $L_S$  by following MoCo v2 [3] as Equation 9 shows. Here  $k_1^-$  are the representations of negative (dissimilar) key samples stored in a queue, e.g., Queue 1 in Figure 6.  $\tau$  is the temperature hyper-parameter, and the default  $\tau = 0.2$  is used, as in [3]. For each query,  $q_1$  and  $k_1$  form a positive pair because they are data-augmented versions of the same image. In contrast,  $q_1$  and  $k_1^-$  form negative pairs since they come from different-class images. After each query,  $k_0$  and  $k_1$  will be appended to Queue 0 and Queue 1 respectively, acting as negative samples in other queries.

$$L_S = -\log \frac{\exp(q_1 \cdot k_1 / \tau)}{\exp(q_1 \cdot k_1 / \tau) + \sum_{k_1^-} \exp(q_1 \cdot k_1^- / \tau)} \quad (9)$$

We formulate our attack in SSL encoder as one optimization problem, i.e., maximizing the similarity between representations  $q_0^t$  and  $k_0^t$ ,  $q_1^t$  and  $k_1^t$ . For this reason, we define local attack loss  $L_L$  and global attack loss  $L_G$  in Equation 10 and Equation 11, respectively.  $q_0^t$  and  $q_1^t$  are representations of the image that is poisoned,  $k_0^t$  and  $k_1^t$  are representations of the image that is a target class, and  $k_0^-$  and  $k_1^-$  are representations of other images which means  $q_0^t$  and  $k_0^t$ ,  $q_1^t$  and  $k_1^t$  form positive pairs whereas  $q_0^t$  and  $k_0^-$ ,  $q_1^t$  and  $k_1^-$  form negative pairs. We use both local attack loss and global attack loss because we consider the local loss helps extract local features but the global loss on the projector's output helps extract additional high-level context information.

$$L_L = -\log \frac{\exp(q_0^t \cdot k_0^t / \tau)}{\exp(q_0^t \cdot k_0^t / \tau) + \sum_{k_0^-} \exp(q_0^t \cdot k_0^- / \tau)} \quad (10)$$

$$L_G = -\log \frac{\exp(q_1^t \cdot k_1^t / \tau)}{\exp(q_1^t \cdot k_1^t / \tau) + \sum_{k_1^-} \exp(q_1^t \cdot k_1^- / \tau)} \quad (11)$$

### B. Average number of queries

Given a ratio  $r$  and an unlabeled training set with  $N$  images including  $N_t$  target-class images, the attacker needs to identify  $PN = N \times r$  target-class images to poison. To identify one target-class image from the unlabeled and disordered dataset, the attacker must go through the whole dataset. We define the process of determining whether an image belongs to the target



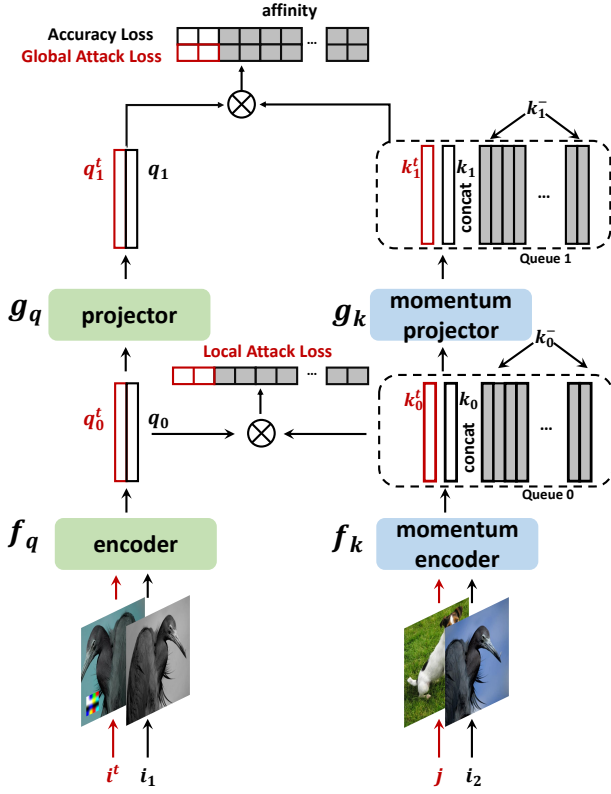


Fig. 6. ESTAS with MoCo v2.

class as a single query. The average number of queries ( $AQ$ ) to get  $PN$  target-class samples is the mathematic expectation of the number of queries.

First, we define  $P(n)$  in Equation 12 to describe the probability that at least  $n$  queries are needed to get  $PN$  target-class images.

$$P(n) = \frac{\binom{N_t}{PN} \cdot \binom{N-N_t}{n-PN}}{\binom{N}{n}} \cdot \frac{PN}{n} \quad (12)$$

The first term of Equation 12, i.e.,  $\frac{\binom{N_t}{PN} \cdot \binom{N-N_t}{n-PN}}{\binom{N}{n}}$  denotes the probability of getting  $PN$  target-class images in  $n$  queries and it can be understood as follows:  $\binom{N}{n}$  denotes the number of methods to draw  $n$  out of  $N$  images;  $\binom{N_t}{PN}$  indicates the number of methods to draw  $PN$  target-class images and  $\binom{N-N_t}{n-PN}$  indicates the number of methods to draw  $n-PN$  out of  $n-PN$  non-target class images. The second term, i.e.,  $\frac{PN}{n}$ , is to ensure that the last image of  $n$  belongs to the target class. Otherwise, it will no longer need  $n$  queries to get  $N_t$  target-class images.

So, we can define  $AQ$  using the following Equation 13 and Equation 14, where  $K$  in Equation 13 and Equation 14 means the worst-case query number. The worst case means that all  $N_t$  target-class images are located in the last  $N_t$  images.

$$AQ = E(n) = \sum_{n=1}^K nP(n) = \sum_{n=1}^K \frac{\binom{N_t}{PN} \cdot \binom{N-N_t}{n-PN}}{\binom{N}{n}} \cdot PN \quad (13)$$

$$K = N - PN + N_t \quad (14)$$

### C. Stability and Attack Efficacy Analysis on Bad-Encoder and our ESTAS

To compare the stability and attack efficacy of our baseline Bad-Encoder and our ESTAS, in Figure 7, we use t-SNE [20] to visualize their representations of poisoned inputs and clean inputs in the test set. Figure 7(a) shows the distribution of representations when attacking a pre-trained clean model with Bad-Encoder[10]. The representations of the poisoned images are not only entangled with the target-class representations, i.e., Tabby Cat, but also entangled with the House Cat and Alley Cat that have similar representations with Tabby Cat in feature space. This is because the clean pre-trained encoder will output similar representations to these categories. This is one of the reasons why Bad-Encoder can occasionally achieve a high  $ASR$  but cannot achieve a stable attack, e.g., it may classify the poisoned image into a non-target class that is similar to the target class. In contrast, when using ESTAS, as Figure 7(b) shows, the encoder generates entangled representations for poisoned images and target-class images. And their representations have a large distance from other-class features that are similar in the Bad-Encoder. One of the reasons is that our ESTAS trains an encoder from scratch, eliminating the reliance on a pre-trained model that is required by our baseline Bad-Encoder for attacks.

### D. Scheduler of hyper-parameters $\lambda_1$ and $\lambda_2$ for multiple-object optimization

$$L_{ESTAS} = L_S + \lambda_1 L_G + \lambda_2 L_L \quad (15)$$

$$\lambda_1, \lambda_2 = \lambda_{10} \cdot \frac{e}{E}, \lambda_{20} \cdot \frac{e}{E} \quad (16)$$

Our ESTAS converts the Trojan attack in the SSL image encoder as a multiple-object optimization problem, i.e., optimizing model accuracy, global attack loss, and local attack loss shown in Equation 15. For this reason, we have two hyper-parameters  $\lambda_1$  and  $\lambda_2$ . We use a linear scheduler to enable stable training. The  $\lambda_1$  and  $\lambda_2$  will change according to current training epochs  $e$  and total training epochs  $E$  as Equation 16 shows. In Equation 16,  $\lambda_{10}$  and  $\lambda_{20}$  are the initial values of  $\lambda_0$  and  $\lambda_1$  which equal to 1.0 as default. And  $\frac{e}{E}$  which means the training progress changes from 0 to 1. By using this scheduler, the model will initially prioritize minimizing accuracy loss and pay increasing attention to minimizing attack loss as training progresses.

### E. Multi-target trojan attack with the same trigger partten

Compared to the inconsistent trigger poison, the consistent trigger poison can ensure that the location of the trigger pattern in the image remains consistent across all training images, but the inconsistent trigger poison cannot. Because the location of triggers added by inconsistent trigger poison will be changed by following data augmentation, but will not be changed if

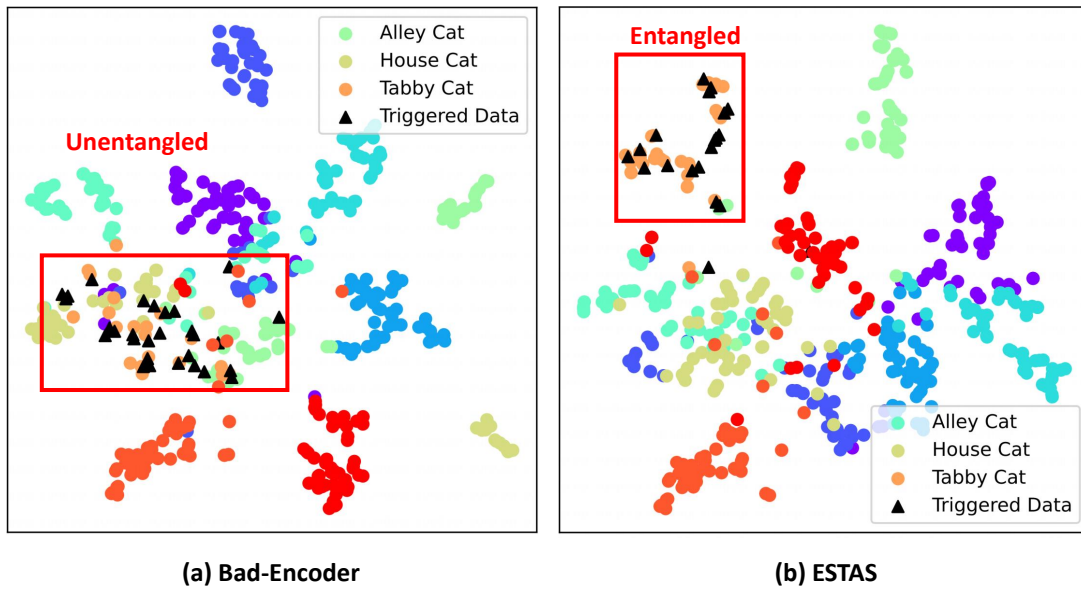


Fig. 7. t-SNE visualization of features in Bad-Encoder.

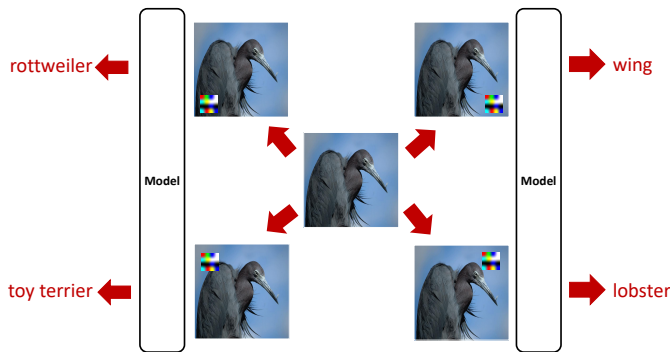


Fig. 8. Multi-target trojan attack.

triggers are added by consistent trigger poison since it adds triggers after data augmentation. For this reason, the model attacked with consistent trigger poison is location sensitive. We have designed the multi-target trojaned model based on this location sensitivity.

In Figure 8, we use the ESTAS to train a trojaned model which will output four different labels when patching the same trigger pattern on the different locations of the same test image. And we can achieve 98.3% *ASR* on average for each target class.

## REFERENCES

- [1] Eugene Bagdasaryan and Vitaly Shmatikov. Blind backdoors in deep learning models. In *30th USENIX Security Symposium (USENIX Security 21)*, pages 1505–1521, 2021. 1, 2, 3
- [2] Ting Chen, Simon Kornblith, Kevin Swersky, Mohammad Norouzi, and Geoffrey Hinton. Big self-supervised models are strong semi-supervised learners. *arXiv preprint arXiv:2006.10029*, 2020. 1, 2
- [3] Xinlei Chen, Haoqi Fan, Ross Girshick, and Kaiming He. Improved baselines with momentum contrastive learning. *arXiv preprint arXiv:2003.04297*, 2020. 1, 2, 5, 6, 8
- [4] Xinlei Chen and Kaiming He. Exploring simple siamese representation learning. *CoRR*, abs/2011.10566, 2020. 2
- [5] Xinyun Chen, Chang Liu, Bo Li, Kimberly Lu, and Dawn Song. Targeted backdoor attacks on deep learning systems using data poisoning. *CoRR*, abs/1712.05526, 2017. 1, 2
- [6] Jia Deng, Wei Dong, Richard Socher, Li-Jia Li, Kai Li, and Li Fei-Fei. Imagenet: A large-scale hierarchical image database. In *2009 IEEE Computer Society Conference on Computer Vision and Pattern Recognition (CVPR 2009)*, 20–25 June 2009, Miami, Florida, USA, pages 248–255. IEEE Computer Society, 2009. 5
- [7] Jean-Bastien Grill, Florian Strub, Florent Altché, Corentin Tallec, Pierre Richemond, Elena Buchatskaya, Carl Doersch, Bernardo Avila Pires, Zhaohan Guo, Mohammad Gheshlaghi Azar, Bilal Piot, koray kavukcuoglu, Remi Munos, and Michal Valko. Bootstrap your own latent - a new approach to self-supervised learning. In H. Larochelle, M. Ranzato, R. Hadsell, M.F. Balcan, and H. Lin, editors, *Advances in Neural Information Processing Systems*, volume 33, pages 21271–21284. Curran Associates, Inc., 2020. 1, 2, 4, 5, 6
- [8] Tianyu Gu, Brendan Dolan-Gavitt, and Siddharth Garg. Badnets: Identifying vulnerabilities in the machine learning model supply chain. *CoRR*, abs/1708.06733, 2017. 1, 2
- [9] Kaiming He, Xiangyu Zhang, Shaoqing Ren, and Jian Sun. Deep residual learning for image recognition. In *2016 IEEE Conference on Computer Vision and Pattern Recognition, CVPR 2016, Las Vegas, NV, USA, June 27–30, 2016*, pages 770–778. IEEE Computer Society, 2016. 5
- [10] Jinyuan Jia, Yupei Liu, and Neil Zhenqiang Gong. Badencoder: Backdoor attacks to pre-trained encoders in self-supervised learning. In *2022 IEEE Symposium on Security and Privacy (SP)*, pages 2043–2059. IEEE, 2022. 2, 3, 4, 7, 9
- [11] Jing Yu Koh. Model Zoo: Discover open source deep learning code and pretrained models. <https://modelzoo.co/>, 2018. [Online; accessed 19-July-2018]. 4
- [12] Soroush Abbasi Koohpayegani, Ajinkya Tejankar, and Hamed Pirsiavash. Compress: Self-supervised learning by compressing representations. In Hugo Larochelle, Marc’Aurelio Ranzato, Raia Hadsell, Maria-Florina Balcan, and Hsuan-Tien Lin, editors, *Advances in Neural Information Processing Systems 33: Annual Conference on Neural Information Processing Systems 2020, NeurIPS 2020, December 6–12, 2020, virtual*, 2020. 8
- [13] Alex Krizhevsky. Learning multiple layers of features from tiny images. 2009. 5
- [14] Alex Krizhevsky, Vinod Nair, and Geoffrey Hinton. Cifar-100 (canadian institute for advanced research). 5
- [15] Changjiang Li, Ren Pang, Zhaohan Xi, Tianyu Du, Shouling Ji, Yuan

- Yao, and Ting Wang. Demystifying self-supervised trojan attacks. *arXiv preprint arXiv:2210.07346*, 2022. [1](#), [2](#), [3](#), [7](#)
- [16] Hongbin Liu, Jinyuan Jia, and Neil Zhenqiang Gong. Poisonedencoder: Poisoning the unlabeled pre-training data in contrastive learning. *arXiv preprint arXiv:2205.06401*, 2022. [1](#), [2](#), [3](#), [4](#), [7](#)
- [17] Yingqi Liu, Shiqing Ma, Yousra Aafer, Wen-Chuan Lee, Juan Zhai, Weihang Wang, and X. Zhang. Trojaning attack on neural networks. In *NDSS*, 2018. [1](#), [2](#), [3](#)
- [18] Aniruddha Saha, Akshayvarun Subramanya, and Hamed Pirsiavash. Hidden trigger backdoor attacks. In *The Thirty-Fourth AAAI Conference on Artificial Intelligence, AAAI 2020, The Thirty-Second Innovative Applications of Artificial Intelligence Conference, IAAI 2020, The Tenth AAAI Symposium on Educational Advances in Artificial Intelligence, EAAI 2020, New York, NY, USA, February 7-12, 2020*, pages 11957–11965. AAAI Press, 2020. [6](#)
- [19] Aniruddha Saha, Ajinkya Tejankar, Soroush Abbasi Koohpayegani, and Hamed Pirsiavash. Backdoor attacks on self-supervised learning. *arXiv preprint arXiv:2105.10123*, 2021. [1](#), [2](#), [3](#), [4](#), [5](#), [6](#), [7](#)
- [20] Laurens van der Maaten and Geoffrey Hinton. Visualizing data using t-SNE. *Journal of Machine Learning Research*, 9:2579–2605, 2008. [9](#)
- [21] Jun Yue, Leyuan Fang, Hossein Rahmani, and Pedram Ghamisi. Self-supervised learning with adaptive distillation for hyperspectral image classification. *IEEE Transactions on Geoscience and Remote Sensing*, 60:1–13, 2022. [8](#)